Oriented nucleation of hemozoin at the digestive vacuole membrane in *Plasmodium falciparum*

Sergey Kapishnikov[a,1], Allon Weiner[a,1], Eyal Shimoni[b], Peter Guttmann[c], Gerd Schneider[c], Noa Dahan-Pasternak[d], Ron Dzikowski[d], Leslie Leiserowitz[a,2], and Michael Elbaum[a,2]

[a]Department of Materials and Interfaces, Weizmann Institute of Science, Rehovot 76100, Israel; [b]Chemical Research Support Department, Weizmann Institute of Science, Rehovot 76100, Israel; [c]Helmholtz Zentrum Berlin für Materialien und Energie GmbH, Wilhelm-Conrad-Röntgen Campus, 12489 Berlin, Germany; and [d]Department of Microbiology and Molecular Genetics, The Kuvin Center for the Study of Infectious and Tropical Diseases, IMRIC, The Hebrew University-Hadassah Medical School, Jerusalem 91120, Israel

Edited by* Ada Yonath, Weizmann Institue, Rehovot, Israel, and approved May 10, 2012 (received for review November 3, 2011)

Heme detoxification is a critical step in the life cycle of malaria-causing parasites, achieved by crystallization into physiologically insoluble hemozoin. The mode of nucleation has profound implications for understanding the mechanism of action of antimalarial drugs that inhibit hemozoin growth. Several lines of evidence point to involvement of acylglycerol lipids in the nucleation process. Hemozoin crystals have been reported to form within lipid nanospheres; alternatively, it has been found in vitro that they are nucleated at an acylglycerol lipid–water interface. We have applied cryogenic soft X-ray tomography and three-dimensional electron microscopy to address the location and orientation of hemozoin crystals within the digestive vacuole (DV), as a signature of their nucleation and growth processes. Cryogenic soft X-ray tomography in the "water window" is particularly advantageous because contrast generation is based inherently on atomic absorption. We find that hemozoin nucleation occurs at the DV inner membrane, with crystallization occurring in the aqueous rather than lipid phase. The crystal morphology indicates a common {100} orientation facing the membrane as expected of templated nucleation. This is consistent with conclusions reached by X-ray fluorescence and diffraction in a companion work. Uniform dark spheres observed in the parasite were identified as hemoglobin transport vesicles. Their analysis supports a model of hemozoin nucleation primarily in the DV. Modeling of the contrast at the DV membrane indicates a 4-nm thickness with patches about three times thicker, possibly implicated in the nucleation.

heterogeneous crystal nucleation | beta-hematin | X-ray microscopy | focused ion beam | quinoline

Malaria is caused by parasites of the *Plasmodium* genus that invade host red blood cells and feed on the hemoglobin. The released heme byproduct Fe(II)-protoporphyrin IX, which is toxic to the parasite, is sequestered by formation of a cyclic dimer (1) linked via reciprocal Fe(III)−O(propionate) bonds, which assembles into physiologically insoluble crystals of hemozoin. Common quinoline drugs against malaria interfere with heme detoxification by inhibiting this process. Extensive evidence points to involvement of acylglycerol lipids in the crystallization of hemozoin. This includes promotion of formation of the synthetic analogue of hemozoin, β-hematin, in acylglycerol suspensions (2) and at various lipid–solution interfaces (3–5), mass spectroscopic analysis of lipids adsorbed on hemozoin crystals isolated from infected RBCs (6), and transmission electron microscopy (TEM) of histologically stained thin sections (6, 7). Within the parasite *Plasmodium falciparum*, hemozoin crystals are found prominently in the DV. Some authors have claimed that hemozoin nucleation occurs within neutral lipid droplets inside the DV (6, 7). Others have suggested that hemoglobin digestion and hemozoin formation may occur primarily in hemoglobin transport vesicles (HTVs) that later fuse with the DV (8), or may be initiated in pre-DV compartments that coalesce to form the mature DV (9), or in a single large engulfment of RBC cytoplasm (10).

Our hypothesis has been that hemozoin nucleates at an acylglycerol lipid–aqueous interface (3–5, 11), based on analogy to the wide literature on templated nucleation (12). A specific expectation is that the relative orientation of mature crystals should reflect their initial nucleation. In the companion report (13), hemozoin alignment was characterized using nanoprobe beam X-ray Fe-fluorescence and crystal diffraction. Crystals were found in clusters with the *c* axis of individual needles aligned in parallel. The diffraction pattern indicated alignment along a curved surface, with {100} faces adjoint to that surface.

To establish the crystal orientation with respect to such lipids, we have here applied real-space electron and X-ray microscopy tools in order to locate the lipid structures possibly implicated in hemozoin nucleation. Cryogenic soft X-ray tomography (cryo-XT) (14) is uniquely suited to examine the above questions because contrast can be interpreted quantitatively. We have applied such analysis in detail to the content of HTVs and to the thickness of the DV membrane. Cryo-XT has been applied recently by others to study stage progression and hemoglobin consumption in *Plasmodium* (15, 16). Working with X-ray illumination energies between atomic absorption transitions of carbon and oxygen, the so-called "water window" from 280 to 530 eV, lipid bodies and dense organic matter appear dark while the aqueous medium is relatively bright. As implemented at the electron storage ring BESSY II (Berlin, Germany), cryo-XT offers in-plane resolution of approximately 30 nm, fully cryogenic sample handling, and 3D reconstruction (14).

The basis for material analysis appears in Fig. 1*A*. The long penetration length of the X-rays in water, reaching 10 μm, permits direct observation of intact cells in the vitrified state and avoids the stages of chemical fixation, dehydration, embedding, staining, and sectioning normally required for electron microscopy. Hemozoin, by virtue of its Fe and high carbon content and density (1.49 g/cm^3), is dark. For reference, the theoretical growth morphology of hemozoin (17) and its spatial relationship to the molecular packing of synthetic hemozoin (1) are depicted in Fig. 1 *B* and *C*.

Author contributions: S.K., A.W., L.L., and M.E. designed research; S.K., A.W., and M.E. performed research; E.S., P.G., G.S., N.D.-P., R.D., and L.L. contributed new reagents/analytic tools; S.K. contributed in cryo-XT; A.W. contributed in EM and preparation for cryo-XT; S.K., A.W., L.L., and M.E. analyzed data; and S.K., A.W., L.L., and M.E. wrote the paper.

The authors declare no conflict of interest.

*This Direct Submission article had a prearranged editor.

Freely available online through the PNAS open access option.

[1]S.K. and A.W. contributed equally to this work.

[2]To whom correspondence may be addressed. E-mail: michael.elbaum@weizmann.ac.il or leslie.leiserowitz@weizmann.ac.il.

This article contains supporting information online at www.pnas.org/lookup/suppl/doi:10.1073/pnas.1118120109/-/DCSupplemental.

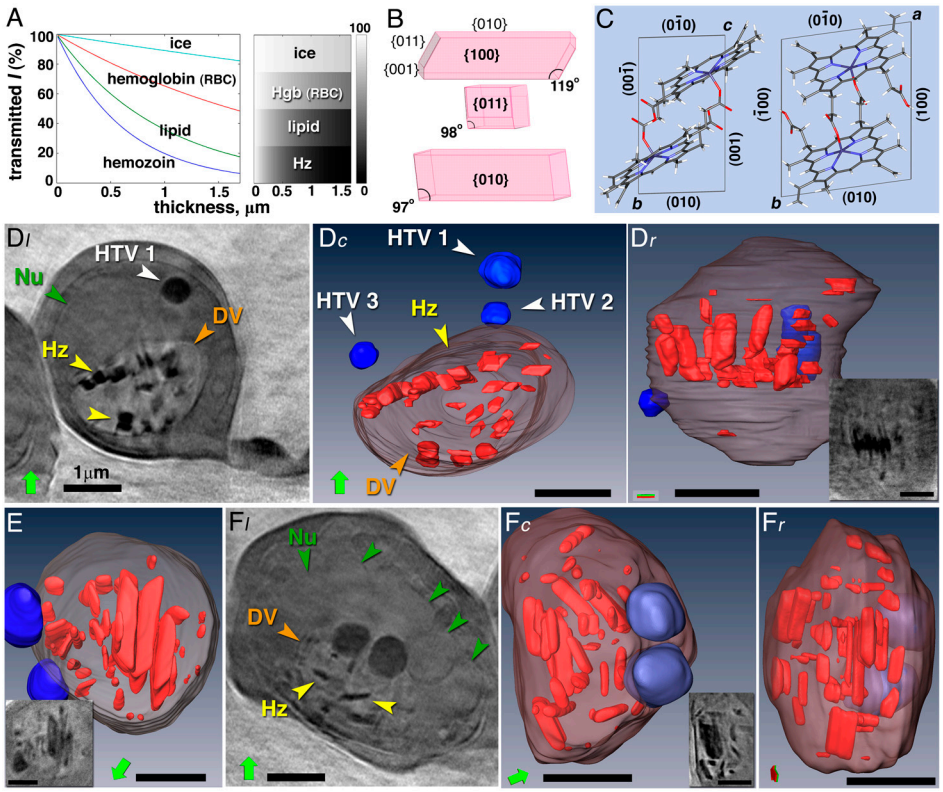

Fig. 1. X-ray cryotomography of hemozoin within *P. falciparum* cells. (*A–C*) For reference: (*A*) relative transmitted intensity at 510 eV energy as a function of material thickness for vitreous ice, cytoplasmic hemoglobin (Hgb), diacylglycerol lipid layer, and hemozoin, together with display gray value; the X-ray absorption coefficients of these materials are, respectively, 0.109, 0.427, 1.031, and 1.618 μm^{-1}. (*B*) Theoretical growth habit of hemozoin, displaying the dominant faces. (*C*) Packing arrangement of synthetic hemozoin. (*D*) Midtrophozoite-stage parasite with a single nucleus (Nu), and large DV enclosing numerous hemozoin (Hz) crystals. (*D*, *l*) A slice through the volume reconstruction; the unreconstructed projection appears in *SI Text*. (*D*, *c* and *r*) Surface renderings from orthogonal view angles of the DV (maroon), Hz (red), and hemoglobin transport vesicles. Note the flattened shape of the DV. (*E*) Surface rendering of a DV from a second late-trophozoite, or perhaps early-schizont, with nearly spherical DV; note the large crystals at the center and the smaller ones lying along the inner membrane. (*F*) Multinuclear schizont-stage parasite with a compacted DV showing Hz crystals primarily at the center. *Insets* show virtual slices through the crystals in the volume reconstructions at similar orientations to those of the respective surface renderings. All scale bars, 1 μm.

Various modes of EM have also been applied. These included freeze-fracture cryo-SEM, serial surface view (SSV) microscopy (18) in a dual-head focused ion beam—scanning electron microscope (19, 20), and scanning transmission electron (STEM) tomography (21). Like the cryo-XT, the latter two offer 3D information, albeit with embedded samples. A glossary of technical terms relating to electron microscopy and *Plasmodium*, as well as experimental details on sample preparation, cryo-XT, and EM, are given in *SI Text*.

Results and Discussion

Hemozoin Distribution in the DV Characterized by Cryo-XT and 3D EM. Infected RBCs in trophozoite and schizont stages were concentrated and vitrified directly on high-tilt tomography grids by high-pressure freezing or plunging to liquid ethane. Representative cryo-XT reconstructions are displayed in Fig. 1 *D–F*. The DV is clearly visible in the cells, as are numerous hemozoin crystals within. Hemozoin crystals in the mononuclear trophozoite (Fig. 1*D*) lie side by side in at least approximate alignment, all in close proximity to the inner membrane surface of the DV. In a later trophozoite stage (Fig. 1*E*), hemozoin clusters appear in the center of the DV, with much smaller crystals lining its inner surface. In the multinuclear schizont (Fig. 1*F*) there are again several clusters of aligned crystals uniformly distributed in the center of the DV, with a number of smaller crystals close to its inner membrane. In no case did we observe any signature of a lipid droplet enveloping the crystals, in contrast to earlier interpretations of electron microscopy of thin sections stained with malachite green (6, 7).

Fig. 2*A* shows an early trophozoite imaged by three-dimensional SSV microscopy. Three-dimensional rendering reveals a flattened, disk-like DV with numerous hemozoin crystals distributed around the inner surface. Fig. 2 *B* shows similar views from a schizont-stage parasite in which the DV has inflated to a more spherical shape. Large crystals fill the interior whereas small crystals are found along the boundary. Fig. 2*C* shows cryo-SEM of a freeze-fracture surface of the DV, again showing hemozoin crystals at the inner membrane. (Like cryo-XT, this technique relies only on physical immobilization by high-pressure freezing.) Fig. 2*D* shows the same phenomenon by STEM tomography.

The location of hemozoin crystals shows a consistent pattern across the various methods of observation. In the earlier stages, clusters of aligned crystals were closely apposed to the DV inner membrane, although at later stages clusters of large crystals were found toward the center of the DV, as quantified in Table S1. Total hemozoin was used as a gauge for parasite age because it reflects the progress of hemoglobin digestion. Early trophozoites, as characterized by EM, also showed somewhat flattened (disk-like) DVs, although later trophozoites and multinuclear schizonts had more spherical DVs. Inflation of the DV through the cell cycle has already been described in detail by electron tomography (9).

In general, where fast and efficient crystal formation would appear to be imperative, as in the case of *Plasmodium*, heterogeneous nucleation is favored over homogeneous. Moreover, growth of an existing crystal is thermodynamically preferred to homogeneous nucleation of a new one. The presence of crystals at the DV membrane in the early trophozoite stages is thus strong evidence for a mechanism of induced nucleation there. Although

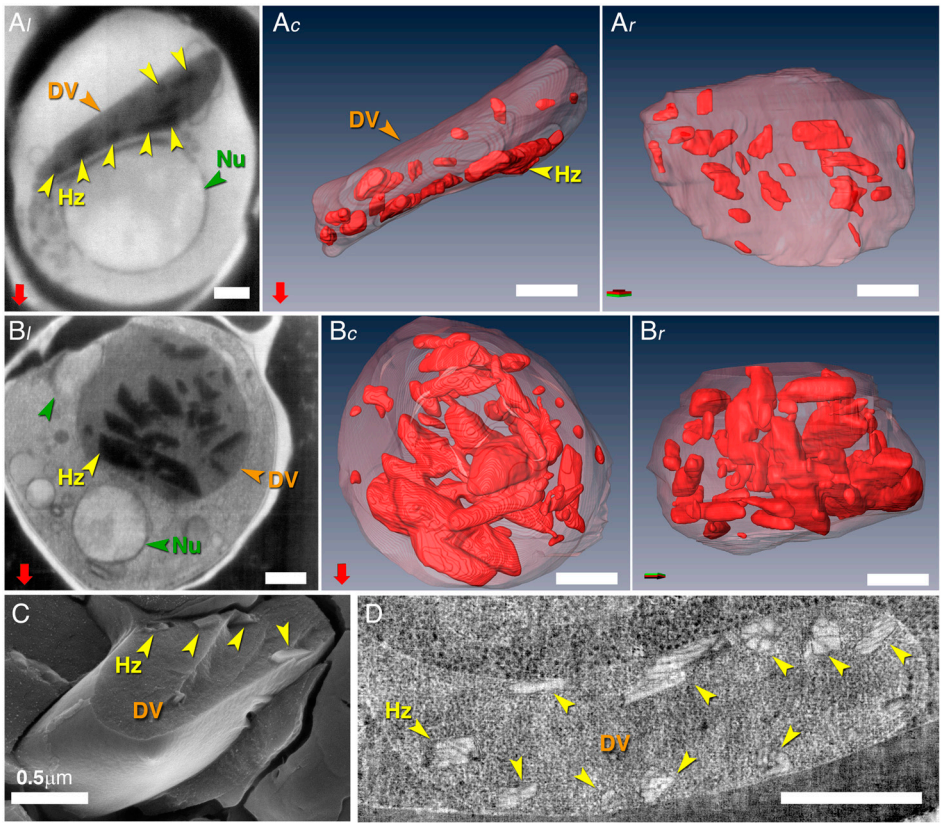

Fig. 2. Electron microscopy of *P. falciparum*. (*A*) SSV EM of a trophozoite-stage parasite: (*A*, *l*) a single section; (*A*, *c* and *r*) surface renderings of the DV displaying hemozoin crystals within (orthogonal views). (*B*) SSV EM of a schizont-stage cell with hemozoin crystals concentrated to the center of the DV. (*C*) Hemozoin crystals lining the DV inner membrane shown by cryo-SEM of a freeze-fracture surface. (*D*) A reconstructed section of the DV by STEM tomography, showing numerous hemozoin crystals lining the inner membrane (yellow arrows). The high contrast obtained by this method reveals cracks within the crystals, possibly along crystallographic planes. Cells in *C* and *D* are from early trophozoites. All scale bars, 0.5 μm.

the methods employed cannot address history of individual cells, we interpret the images in toto to indicate that crystals are nucleated at the DV membrane and later leave it. A nucleating template lowers the surface free energy for growth of a particular face of the crystal, and therefore the orientation facing the membrane is of great significance. Our model is that clusters form with roughly parallel needle axes, which over time break away from the membrane. This process is possibly assisted by the change in membrane curvature upon inflation of the DV. Thus, the largest crystals at the center of the schizont DV are also likely the oldest. Other possibilities may exist—e.g., different growth rates for membrane-bound and free crystals, or delivery of preformed crystals from transport vesicles (*vide infra*). However, it is difficult to see how these effects could lead to a consistent relative orientation of neighboring crystals around the needle axis in a cluster, so we focus on this question in the following section.

Orientation of Hemozoin Crystals *vis-à-vis* the DV Membrane Surface. We now examine in comprehensive detail the oriented alignment of crystals adjacent to the DV membrane, using Fig. 1*B* as a guide for crystal morphology. Fig. 3*A* shows a section from STEM tomography reconstruction with five oriented crystals. The needle *c* axes lie in parallel, while obtuse vertex angles close to 120° indicate that the crystals expose the same {100} face. We may suspect that these crystals were nucleated along a lipid surface that lay outside the section, or that they detached together from the nucleating surface. Had the crystals simply packed together along flat facets after formation, we would expect to see both 120° and 95° vertices indicating exposed {100} and {010} faces. Other examples of mutual orientation appear in the freeze-fracture images of Fig. 3 *Bl* and *Bc*, again with {100} faces exposed. Note that the neighboring hemozoin crystals in Fig. 3*Bc* are not in contact, yet all expose the {100} face; this shows that the common orientation around the *c* axis precedes crystal agglomeration. Note also that the two crystals in Fig. 3*Bl* as well as crystals in Fig. S1 expose (100) and $(\bar{1}00)$ faces, the surface structures of which are chiral and of opposite handedness. Clearly one crystal could not have been nucleated from the other via their adjacent {010} side faces because of structural misregistry. Fig. 3*Br* shows a trophozoite DV with smaller crystals lying directly at the membrane. The vertex angles indicate a {010} face in view, implying that a {100} face adjoins the membrane, seen edge-on. Three-dimensional imaging confirmed that crystals lie with the long axis parallel to the DV membrane. Fig. 3 *C–F* shows DVs from Fig. 1 with virtual cuts taken parallel to the membrane as indicated. The oblong shape and obtuse vertex angles close to 120° again show both (100) and $(\bar{1}00)$ orientations facing the membrane, demonstrating very weak chiral discrimination. All in all, it is highly unlikely that such mutually oriented crystals would appear together unless a common template had been involved in their nucleation. These interpretations are in full agreement with X-ray diffraction reported in the companion paper (13), as well as with selected 2D EM images from the literature (e.g., figure 2*C* of ref. 22, figure 6*F* of ref. 23, reprinted as Fig. S2, as well as figure 3*D* of ref. 24.

Analysis of Lipid in the DV and DV Membrane. An original motivation in adopting soft X-ray microscopy was to locate the acyl lipid structures or bodies thought to be involved in hemozoin nucleation. The anticipated alternatives were nucleation either within lipid nanospheres, or on the surface of a lipid film. In Fig. 1 we see that the crystals are generally well-formed and sharply delineated. In tomographic reconstruction, contrast represents primarily differences in the X-ray absorption coefficients. Had the crystals been surrounded by a lipid droplet we would have expected to see that lipid. Fig. 4*A* and Fig. S4 show comparisons of relative contrast for hemozoin on the observed background in the DV, as well as on hypothetical carbon densities corresponding to 10–100% of that in an acyl lipid drop. It would be well-nigh impossible to visualize the crystals engulfed within a lipid sphere. In order to confirm the absence of a lipid droplet independently of the reconstruction, we modeled a projection through hemozoin and surrounding lipid, as shown in Fig. 4*B* and Fig. S3

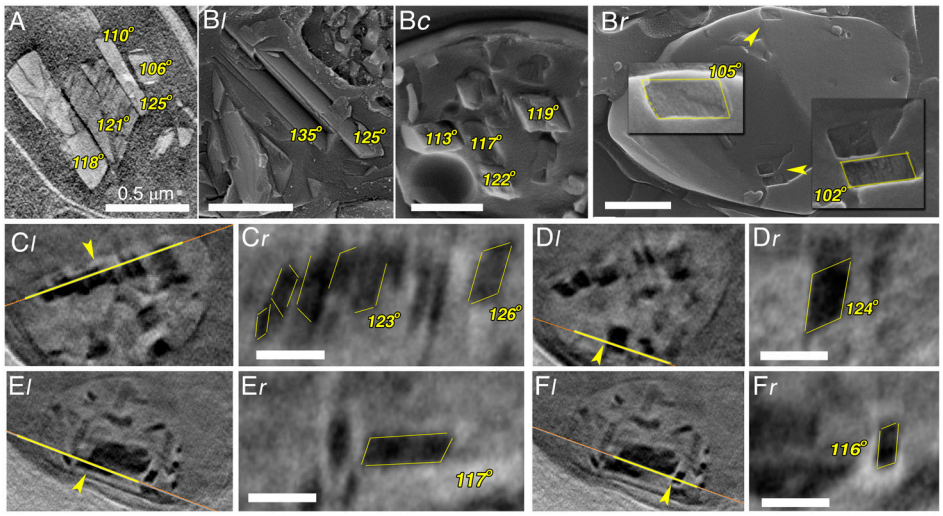

Fig. 3. Analysis of hemozoin crystal morphology indicates orientation at the DV membrane surface. (*A*) A slice through STEM tomography reconstruction showing laterally oriented crystals. (*B*) Freeze-fracture cryo-SEM. (*B*, *l*) Two aligned crystals exposing (100) and ($\bar{1}$00) orientations—namely, with opposite surface structure handedness. (*B*, *c*) Several separated crystals exposing {100} faces, suggesting a common nucleation template. (*B*, *r*) Hemozoin crystals, shown magnified (*Insets*), oriented adjacent to the DV membrane with the long axis lying alongside it; the smaller vertex angles are indicative of {010} orientation in view, implying that {100} lies in contact with the lipid membrane. (*C*–*F*) Slices through the cryo-XT reconstruction parallel to the membrane cut the crystals along the long axis and reveal a common orientation with the *c* axes lying in parallel. Vertex angles indicate {100} orientation adjoining the membrane: (*C*, *D*) trophozoite; (*E*, *F*) schizont. All scale bars, 0.5 μm.

and described in detail in *SI Text*. Again, the crystals are clearly not engulfed in any lipid sphere.

We conclude that a lipid phase of comparable dimension to that of the crystals can be ruled out because of the unique sensitivity of X-ray microscopy in the water window. A thin lipid layer might still be present between adjacent interfaces (2). We propose that earlier evidence for lipid nanospheres surrounding hemozoin (6, 7) might be reinterpreted as crystals in contact with a lipid patch on the DV membrane. Indeed, the crystals shown in those images are oriented exposing their {100} faces (see figure 1*B* in ref. 6 and figure 4 in ref. 7), in keeping with induced nucleation at the membrane surface.

Crystalline orientation with respect to the adjacent membrane strongly suggests that the lipid headgroups serve as a template for nucleation. This effect is well known in many chemical systems (12). However, phospholipid head groups are an unlikely chemi-

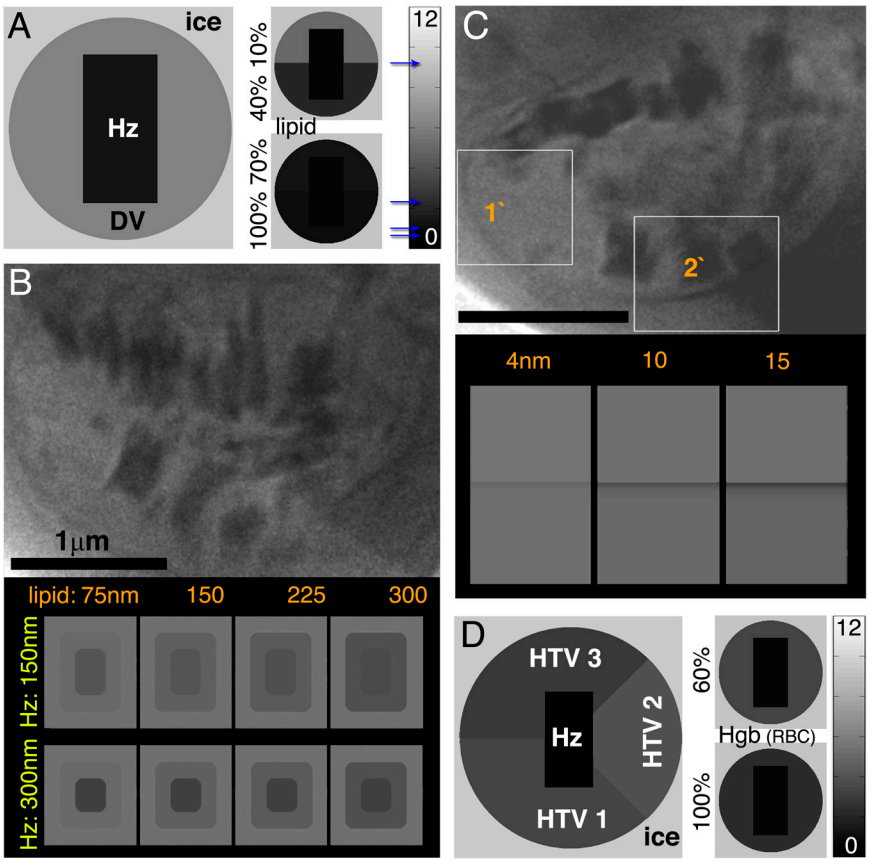

Fig. 4. Detection or absence of lipids by cryo-XT. (*A*) The average contrast intensity of the Hz crystals, their immediate surroundings, and vitreous ice as observed in the reconstruction of the trophozoite in Fig. 1*D*. The intensities are scaled to that of the X-ray attenuation lengths (in μm), the range of which (0–12) is shown along the vertical scale bar together with the relative positions for Hz (0.618), lipid (0.97), cytoplasm hemoglobin (2.33), and vitreous ice (9.2). Four hypothetical hemispheres surrounding the Hz crystals, which simulate 100%, 70%, 40%, and 10% lipid content, are shown for comparison. (*B*) A tilted projection view from the dataset that generated Fig. 1*D* shows the hemozoin crystals side-on. A simulation (*Lower*) of the transmitted contrast through crystals and lipid demonstrates that a lipid envelope of comparable dimension would have generated significant contrast in the projection. (*C*) The untilted view shows varied contrast around the DV membrane (e.g., boxes 1′ and 2′). Modeling indicates a membrane thickness ranging from 4–15 nm (*SI Text*), consistent with patches of lipid lining the defining phospholipid membrane. (*D*) The average intensity values of the three HTVs in Fig. 1*D* are displayed, together with that of Hz and vitreous ice. HTV contrasts correspond to 76%, 59%, and 46% of nominal RBC cytoplasm content. Two hypothetical spheres simulating 100% and 60% cytoplasmic hemoglobin content are shown for comparison. All scale bars, 1 μm.

cal nucleant of hemozoin, and do not promote oriented nucleation of β-hematin in vitro (25). Acylglycerols exposing OH and C=O headgroups induce β-hematin nucleation via its {100} faces (4). There exists a partial stereochemical match in that orientation, depicted in Fig. S8, which is absent for the {010} faces. Therefore, we searched for clues regarding additional lipids on the DV membrane. In the reconstructed section shown in Fig. 1*Dl*, we note a thickening around parts of the DV perimeter, with higher contrast even than the nuclear envelope. (The latter is composed of two juxtaposed phospholipid bilayers—i.e., double the anticipated thickness of the DV.) Fig. 4*C* and Fig. S5 show the untilted projection from the same dataset, confirming that the variability in contrast around the DV is intrinsic and not somehow an artifact of the reconstruction. However, the X-ray imaging resolution is insufficient to resolve membrane thickness directly. In order to interpret the image we modeled the DV as a thin cylindrical lipid shell immersed in water, and simulated the projected image contrast as a function of membrane thickness. (The method is described in *SI Text* and confirmed using the nuclear envelope as a standard, making use of Fig. S6.) We see first that a 4-nm thick membrane should indeed be visible even at 30-nm imaging resolution because of the accumulated absorption along the wall edge. By comparison with the simulated contrast we find that the DV membrane ranges in thickness from 4–16 ± 2 nm. (This computed variation is model-dependent but clearly reaches thicknesses greater than that compatible with a simple phospholipid bilayer.) The extra thickness might be explained by a thin lipid layer coating the membrane from within, and we propose that this might be the active site of hemozoin-nucleating acylglycerol lipid, although we cannot exclude the possibility that the acylglycerol molecules may also be part of the inner leaflet of the membrane. It is possible that local activity of phospholipases generates the acyl lipid involved in hemozoin nucleation (6, 26).

Hemoglobin Uptake, Dark Vesicles Outside the DV, and Hemozoin Nucleation. In each specimen we see a small number of prominent, dark spheres outside the DV (e.g., Fig. 1 *D–F*). The three dark spheres in Fig. 1*D* lie distant from the trophozoite DV, whereas in the late trophozoite (Fig. 1*E*) and the schizont shown in Fig. 1*F*, the spheres appear attached to the DV. Such spheres have been identified in previous works as lipid droplets (2, 16, 23), or, alternatively, as hemoglobin-containing extra-DV compartments (9, 15). For example, the diameter of the three dark spheres in Fig. 1*D* is 410 ± 80 nm, matching that of three vesicles exhibiting dark contrast in the trophozoite XT image reported by Hanssen et al. (330 ± 70 nm) (figure 2*A–C* in ref. 15). We have tried to establish the contents of the dark spheres in Fig. 1 from their X-ray attenuation lengths, limiting our analysis to samples (Fig. 1 *D* and *F*) that were vitrified by high-pressure freezing. After fixing the linear scale with the attenuation lengths of vitrified water in the background and of hemozoin crystals in the DV, contrast in these spheres represents attenuation lengths ranging from 2.9 to 4.5 μm. For comparison, the attenuation length of lipid is estimated to be 1.62 μm. Hypothetical lipid–water spheres would incorporate an unrealistically low lipid content of 26% and 12%, respectively. Moreover, each vesicle has a different contrast, which is inconsistent with a homogeneous lipid composition. On the other hand, given a computed X-ray attenuation length for molecular hemoglobin of 0.56 μm (Fig. S7), which matches perfectly to a recent measurement (16), the derived attenuation lengths correspond to hemoglobin concentrations ranging between 3.8 and 1.8 mM. These values represent 76% and 36%, respectively, of the nominal 5-mM hemoglobin concentration in the cytoplasm of an uninfected RBC. Thus, we interpret these dark spheres in Fig. 1 *D–F* as hemoglobin transport vesicles (8–10, 23, 27, 28), marked as HTV in Fig. 1 and Fig. S5.

It has been shown that hemozoin nucleation may occur within HTVs after DV formation (9), as had been proposed earlier by Hempelmann et al. (8). This might be a source of small crystals unassociated with membranes in the early trophozoites. Taken to the extreme, however, this view suggests that the DV may act simply as a dump for preformed crystals throughout the life cycle. This would conflict with our assertion of nucleation at the DV membrane. Therefore, we tried to find crystals in the observed HTVs, but none were detected. We estimated the size of the largest single crystal that might be formed given the quantity of enclosed hemoglobin, approximately $50 \times 50 \times 180$ nm^3 (as elaborated in *SI Text*). Crystals of this size and smaller were observed inside the DV but not in the HTV, the dark image contrast of which further indicates that X-ray dense hemoglobin had not been depleted. Other arguments speak against pronounced hemozoin crystallization in HTVs. For instance, much smaller crystals could form from the same source of heme; these, upon transfer into the DV, would greatly exceed the number of crystals observed there, about 40 ± 20 according to Table S1. The physiological insolubility of hemozoin implies insignificant Ostwald ripening (growth of large crystals at the expense of smaller ones). We deduce below (*vide infra*) that the number of HTVs is possibly in the hundreds, so the number of crystals in the DV should have been at least comparable. Moreover, in the DV the typical crystal size is much larger than the largest crystal that could form in a transport vesicle (more than an order of magnitude in volume: $130 \times 130 \times 450$ nm^3, as described in *SI Text*). Therefore, significant growth of individual hemozoin crystals must occur in the DV, requiring a delivery of fresh heme from the transport vesicles. This, too, argues against the notion of predominant crystallization within the HTV.

It is also of interest to compare the number of transport vesicles (of the size observed) required to deliver the cellular hemoglobin to the DV with the number required to supply the DV membrane by fusion. Up to 70% of the host hemoglobin is consumed by the parasite in the DV, generating hemozoin (29). Thus, the amount of hemoglobin transported by the HTVs would require a number of vesicles on the order of the ratio of 70% of the RBC-to-HTV volumes—e.g., 0.7×90 μm^3 and 0.075 μm^3, respectively (i.e., approximately 840). Such traffic would carry a lipid surface of approximately 720 μm^2, which exceeds the surface area of the DV, ≅ 20 μm^2, by a large factor. This discrepancy implies a large turnover of lipid at the DV, which has indeed been described (27). Therefore, given the extent of the HTV/DV fusion process and the dynamic nature of the DV membrane, lipid patches of extra thickness (*vide supra*) might well be expected.

Materials and Methods

For X-ray tomography, samples were first pelleted and spread onto high-tilt tomography grids. Grids were then either blotted and plunged to liquid ethane, or, preferably, sandwiched between stainless-steel shims and subjected to high-pressure freezing (HPM-010; Bal-Tec). Cryotomography was performed at the U41 beamline of BESSY II (14). For cryo-SEM imaging, sample pellets were high-pressure frozen between aluminum platelets, then freeze fractured (BAF 60; Bal-Tec), coated with Pt, and transferred to the microscope equipped with a cryogenic sample stage (Ultra 55; Zeiss). For serial surface view microscopy, high pressure—frozen samples were freeze-substituted to Epon and cut to pyramids for introduction into the dual-beam FIB-SEM instrument (Helios 600; FEI) (20). For STEM tomography, similar freeze-substituted material was sectioned to a thickness of approximately 300 nm and imaged in scanning mode using a high-angle dark-field detector in the TEM (Tecnai F20; FEI). Image simulation and quantitative interpretation were based on custom software written in Matlab. Complete details appear in *SI Text*.

Conclusions

We have shown that hemozoin crystals nucleate in an oriented manner at the inner surface of the *Plasmodium* DV. In full agreement with the companion paper's conclusions based on X-ray fluorescence and diffraction, we found that the needle *c* axis of the crystals lies parallel to the DV membrane. All the morphological evidence identifies the {100} side faces of hemozoin as the

one in contact with the lipid interface, and therefore the one most likely to seed nucleation heterogeneously at the DV inner membrane. There appears to be no chiral discrimination between the membrane surface—oriented (100) and ($\bar{1}$00) faces, which are of opposite handedness. A model calculation based on variation in contrast intensity of the X-ray projection image through the DV membrane yielded a thickness of 4 nm with patches up to threefold thicker. We have not observed hemozoin crystals within the hemoglobin transport vesicles en route to the DV; indeed, analysis indicates that very few crystals could have been transferred by such a pathway. Based on the evidence presented, we propose that hemozoin crystals form on an acylglycerol lipid film adsorbed to the inner leaflet of the DV phospholipid membrane. However, acylglycerol molecular patches might also be part of the inner leaflet of the membrane. Nucleation may be appreciated in terms of a stereochemical interaction between the {100} faces and the glycerol headgroups of the lipid surface. Comprehensive analysis of the cryo-XT data rules out the notion of hemozoin crystals being nucleated within lipid nanospheres, or indeed on their surfaces, although a molecularly thin lipid layer may well remain between adjacent crystal interfaces.

An important implication of our findings is that hemozoin crystals grow within the aqueous phase. This solves a paradox in understanding the mechanism of action of water-soluble antimalarial drugs, such as the quinolines, which would hardly function within the lipid droplet. Sequestration of the heme monomer or dimer in solution requires a high stoichiometry of drug to heme, whereas disruption of hemozoin crystal nucleation or growth via a stereoselective drug-to-surface attachment (11, 17, 30) requires only a very low stoichiometry (1) consistent with therapeutic action.

ACKNOWLEDGMENTS. The authors thank Thanat Chookajorn for stimulating discussions, Hagai Ginsburg for a critical reading of the manuscript, Jens Als-Nielsen for both discussions and a reading of the manuscript, Stefan Heim for control software of the X-ray microscope, and Bernard Heymann for advice on tomographic reconstruction using Bsoft. Electron microscopy was conducted at The Irving and Cherna Moscowitz Center for Nano and Bio-Nano Imaging of the Weizmann Institute of Science. This research was made possible by the historical generosity of The Harold Perlman family, The Helen and Milton A. Kimmelman Center for Biological Structure and Assembly, The Gerhardt M.J. Schmidt Minerva Center for Supramolecular Architecture, and The Minerva Research Foundation. A.W. was supported in part by the Curwen-Lowey Fellowship of the Clore Center for Biological Physics. We acknowledge the Helmholtz-Zentrum Berlin Electron Storage Ring BESSY II for provision of synchrotron radiation at beamline U41, with funding from the European Community's Seventh Framework Programme (FP7/2007–2013) under Grant Agreement 226716.

1. Pagola S, Stephens WP, Bohle DS, Kosar AD, Madsen SK (2000) The structure of malaria pigment (β-haematin). *Nature* 404:307–310.
2. Jackson KE, et al. (2004) Food vacuole-associated lipid bodies and heterogeneous lipid environments in the malaria parasite *Plasmodium falciparum*. *Mol Microbiol* 54:109–122.
3. Egan TJ, et al. (2006) Haemozoin (β-haematin) biomineralization occurs by self-assembly near the lipid/water interface. *FEBS Lett* 580:5105–5110.
4. de Villiers KA, et al. (2009) Oriented nucleation of β-hematin crystals induced at various interfaces: Relevance to hemozoin formation. *Cryst Growth Des* 9:626–632.
5. Huang AN, et al. (2010) Crystallization of synthetic haemozoin (β-haematin) nucleated at the surface of lipid particles. *Dalton Trans* 39:1235–1244.
6. Pisciotta JM, et al. (2007) The role of neutral lipid nanospheres in *Plasmodium falciparum* haem crystallization. *Biochem J* 402:197–204.
7. Coppens I, Vielemeyer O (2005) Insights into unique physiological features of neutral lipids in apicomplexa: From storage to potential mediation in parasite metabolic activities. *Int J Parasitol* 35:597–615.
8. Hempelmann E, Motta C, Hughes R, Ward SA, Bray PG (2003) *Plasmodium falciparum*: Sacrificing membrane to grow crystals? *Trends Parasitol* 19:23–26.
9. Abu Bakar N, Klonis N, Hanssen E, Chan C, Tilley L (2010) Digestive-vacuole genesis and endocytic processes in the early intraerythrocytic stages of *Plasmodium falciparum*. *J Cell Science* 123:441–450.
10. Elliott DA, et al. (2008) Four distinct pathways of hemoglobin uptake in the malaria parasite *Plasmodium falciparum*. *Proc Natl Acad Sci USA* 105:2463–2468.
11. Weissbuch I, Leiserowitz L (2008) Interplay between malaria, crystalline hemozoin formation and antimalarial drug action and design. *Chem Rev* 108:4899–4914.
12. Kuzmenko I, et al. (2001) Design and characterization of thin films architectures at the air–liquid interface: Simplicity to complexity. *Chem Rev* 101:1659–1696.
13. Kapishnikov S, et al. (2012) Aligned hemozoin crystals on a curved surface in malarial red blood cells revealed by nanoprobe X-ray Fe-fluorescence and diffraction. *Proc Nat'l Acad Sci USA* 109:11184–11187.
14. Schneider G, et al. (2010) Three-dimensional cellular ultrastructure resolved by X-ray microscopy. *Nat Methods* 7:985–987.
15. Hanssen E, et al. (2011) Cryo transmission X-ray imaging of the malaria parasite *P. falciparum*. *J Struct Biol* 173:161–168.
16. Hanssen E, et al. (2012) Soft X-ray microscopy analysis of cell volume and hemoglobin content in erythrocytes infected with asexual and sexual stages of *P. falciparum*. *J Struct Biol* 177:224–232.
17. Buller R, Peterson ML, Almarsson O, Leiserowitz L (2002) Quinoline binding site on malaria pigment crystal: Rational pathway for antimalarial drug design. *Cryst Growth Des* 2:553–562.
18. Denk W, Horstmann H (2004) Serial block-face scanning electron microscopy to reconstruct three-dimensional tissue nanostructure. *PLoS Biol* 2:e329.
19. Heymann JA, et al. (2006) Site-specific 3D imaging of cells and tissues with a dual beam microscope. *J Struct Biol* 155:63–73.
20. Weiner A, et al. (2011) 3D nuclear architecture reveals coupled cell cycle dynamics of chromatin and nuclear pores in the malaria parasite *Plasmodium falciparum*. *Cell Microbiol* 13:967–977.
21. Hohmann-Marriott MF, et al. (2009) Nanoscale 3D cellular imaging by axial scanning transmission electron tomography. *Nat Methods* 6:729–731.
22. Goldberg DE, Slater AFG, Cerami A, Henderson GB (1990) Hemoglobin degradation in the malaria parasite *Plasmodium falciparum*: An ordered process in a unique organelle. *Proc Natl Acad Sci USA* 87:2931–2935.
23. Dluzewski AR, et al. (2008) Formation of the food vacuole in *Plasmodium falciparum*: A potential role for the 19 kDa fragment of merozoite surface protein 1 (MSP119). *PLoS One* 3:e3085.
24. Sachanonta N, et al. (2011) Ultrastructural and real-time microscopic changes in *P. falciparum-infected* red blood cells following treatment with antimalarial drugs. *Ultrastruct Pathol* 35:214–225.
25. Solomonov I, et al. (2007) Crystal nucleation, growth and morphology of the synthetic malaria pigment β-hematin and the effect thereon by quinoline additives: The malaria pigment as a target of various antimalarial drugs. *J Am Chem Soc* 129:2615–2627.
26. Pisciotta JM, Sullivan DJ (2008) Hemozoin: Oil versus water. *Parasitol Int* 57:89–96.
27. Yayon A, Timberg R, Friedman S, Ginsburg H (1984) Effects of chloroquine on the feeding mechanism of the intraerythrocytic human malarial parasite *Plasmodium falciparum*. *J Protozool* 31:367–372.
28. Slomianny C (1990) Three-dimensional reconstruction of the feeding process of the malaria parasite. *Blood Cells* 16:369–378.
29. Tilley L, Dixon MWA, Kirk K (2011) The *Plasmodium falciparum*—infected red blood cell. *Int J Biochem Cell Biol* 43:839–842.
30. Sullivan DJ, Gluzman IY, Russell DG, Goldberg DE (1996) On the molecular mechanism of chloroquine's antimalarial action. *Proc Natl Acad Sci USA* 93:11865–11870.